Origin of the 3.331 eV emission in ZnO nanorods: comparison of vapour phase transport and pulsed laser deposition grown nanorods

Saikumar Inguva, Ciarán Gray, Enda McGlynn* , Jean-Paul Mosnier*

School of Physical Sciences and National Centre for Plasma Science and Technology,

Dublin City University, Glasnevin, Ireland.

*Corresponding authors: saikumar.inguva2@mail.dcu.ie and enda.mcglynn@dcu.ie.

KEYWORDS

ZnO seed layers, vertically aligned ZnO nanorods, vapour phase transport, pulsed laser deposition, 3.331 eV emission.

ABSTRACT

In this work, we report the growth of vertically aligned ZnO nanorods with excellent optical quality by both catalyst free vapor phase transport (VPT) and catalyst free pulsed laser deposition (PLD). We compare the near band edge emission of such deposits, with a focus on the identification of the origin of the 3.331 eV emission feature. X-ray diffraction (XRD), scanning electron microscopy (SEM) and low-temperature (13 K) photoluminescence (PL) were used to characterise these nanorod deposits. XRD and SEM data reveal that both techniques lead to highly textured ZnO nanorod arrays with uniform *c*-axis orientation normal to the substrate surface. The VPT-grown nanorods are well separated and show smooth, facetted surfaces whereas the PLD-grown nanorods are more closely packed and display comparatively rougher surfaces. The optical quality of the samples obtained by both growth methods was very good and low-temperature PL spectra were dominated in both cases by a strong I_6 bound exciton (BX) emission (3.36 eV), and also showed emission from the surface exciton and the free exciton. A comparatively weak visible emission was also observed in samples deposited by both techniques. The main difference between the PLD- and VPT-grown nanorod samples is the presence of the 3.331 eV emission in the former, and its complete absence in the latter (as well as in continuous PLD-grown seed layers) which is discussed in light of the differing surface morphologies mentioned above and which provides strong support for our previous assignment of the origin of this defect to structural defects in the inhomogeneous sub-surface region close to the rough nanorod surface.

1. Introduction

ZnO has a range of promising material properties including a wide direct band gap (3.37 eV) and a large exciton binding energy (60 meV) [1]. Furthermore, low dimensional ZnO single crystal nanostructures can be grown in a variety of morphologies with excellent crystalline quality and optical properties [1]. This has resulted in considerable interest in the growth of ZnO based nanostructures such as nanorods, nanowires and nanobelts. Amongst this range of morphologies, vertically aligned ZnO nanostructures (1D) have been of particular interest because this morphology is especially well suited to potential applications in optoelectronic devices (as it enables efficient electrical contacting of arrays of nanorods) and in field emission devices [2-4].

Many deposition techniques including vapour phase transport (VPT) [5-9], metal-organic chemical vapour deposition (MOCVD) [1,10], hydrothermal deposition [11], pulsed laser deposition (PLD) [12], electrochemical deposition [13], and chemical bath deposition (CBD) [14] have been used to grow vertically aligned ZnO nanorods with good crystalline quality and optical properties.

The utilisation of ZnO nanorods in optoelectronic devices is ultimately determined by the optical quality of the nanorods [3]. Thus an understanding of the different optically-active defects which contribute to the near-UV band edge photoluminescence (PL) in ZnO and its nanostructures and the relationship of these defects to the nanostructure morphology is key to the choice of the optimum deposition methods and conditions for a particular application. In this work we have grown ZnO nanorods by catalyst free VPT and catalyst free PLD, and characterised these deposits by x-ray diffraction (XRD), scanning electron microscopy (SEM) and low-temperature photoluminescence (PL), with the aim of further elucidating the origin of

the recently reported 3.331 eV defect emission [12]. Comparison of the near band edge PL emission of the nanorod deposits grown by both PLD and VPT shows that the 3.331 eV emission is present in the former and completely absent in the latter (and also absent in the continuous PLD-grown seed layers). These data are considered in light of SEM data showing smooth, facetted VPT-grown nanorod surfaces, compared to rougher PLD-grown nanorod surfaces and provides strong support for the previous assignment of the origin of the recently observed 3.331 eV emission to structural defects in the inhomogeneous sub-surface region close to the rough nanorod surface.

2. Experimental details

2.1 ZnO Seed Layer Formation

ZnO seed layers were first prepared by PLD on Si (100) substrates for both VPT and PLD nanorod depositions. Prior to deposition, Si substrates were cleaned by ultrasonication firstly in acetone and then in isopropanol for 15 min each. The PLD apparatus was equipped with a high power, Q-switched, frequency-quadrupled Nd:YAG laser. The wavelength output 266 nm, repetition rate 10 Hz, pulse width 6 ns, laser energy 150 mJ and number of laser shots 5000 were used. The average laser fluency on the ZnO target (99.999%, PI-KEM) was fixed at 2 J/cm^2 and the target-substrate distance was also kept constant at 5 cm. The base pressure of the system was at 6×10^{-5} mTorr while the deposition was carried out at an oxygen pressure of 100 mTorr. Before deposition, for the purpose of surface cleaning, the Si substrate was heated to 950 °C for 30 min and then cooled to 450 °C for 35 min. The deposition was then performed at this temperature. In order to achieve a better crystalline/textured seed layer after the deposition, the seed layer substrate was annealed to 750 °C for 20 min and then cooled back to

150 °C for 60 min. The thickness of the ZnO seed layers was measured to be ~ 120 nm. Further details are given in reference [12].

2.2 VPT Nanorod Growth

ZnO nanorods were grown by VPT on these ZnO-seeded Si substrates at 900 °C using an Ar gas flow rate of 90 sccm for 1 hour. The temperature ramping of the furnace was varied between 25 and 50 °C/min till the temperature reached to 900 °C. 60 mg of high purity graphite powder and 60 mg of ZnO powder were ground together for a few minutes until a homogeneous mixture was obtained. This mixture was then loaded and spread carefully over a 2 cm length in a middle of alumina boat and the sample suspended above it. This boat was then loaded into the furnace for the nanorod growth. Further details concerning the growth process are reported elsewhere [5,6,15].

2.3 PLD Nanorod Growth

ZnO nanorods were also grown by PLD on the ZnO seeded Si substrates described in section 2.1. Prior to deposition, the seed layers were annealed to 800 °C for 110 min. The ZnO nanorods were then grown at this substrate temperature in a 600 mTorr oxygen pressure using 40,000 laser shots for the deposition over a period of ~ 2 hrs. The laser specifications were the same as for the seed layer growth, described in section 2.1. After deposition, the substrate was cooled to 150 °C for 75 min. Further details on the PLD nanorod growth are reported elsewhere [12].

2.4 Deposit Characterisation

The structural characteristics of the deposited materials were investigated by 2θ-ω XRD (Bruker AXS D8 Advance). Surface morphologies were studied by SEM (Carl-Zeiss EVO series). Low-temperature photoluminescence (PL) spectra were recorded using He−Cd laser

excitation at 325 nm with a 1 metre SPEX 1704 monochromator coupled to a Hamamatsu model R3310-02 photomultiplier tube which was cooled to approximately −20 °C.

3. Results and discussion

3.1 Structural properties

XRD data (2θ-ω scans) from PLD-grown ZnO seed layers, VPT-grown ZnO nanorods and PLD-grown ZnO nanorods in addition to data from a *c*-plane terminated ZnO single crystal wafer (Tokyo Denpa) of thickness 0.5 mm are shown in Fig. 1. All the deposited material shows a dominant ZnO (002) reflection at $2\theta \approx 34.5^{o}$. Since the XRD data shown in Fig. 1 is plotted on log scale, a weak ZnO (004) reflection was also observed at $2\theta \approx 72.80^{o}$ in both the seed layer and nanorod samples (shown in the right hand side inset). No other ZnO-related diffraction peaks were observed, which indicates a high degree of texture (vertical orientation) for all the deposited materials. Furthermore, since no catalyst was used in our growth methods, no other deposited material or crystalline phases are observed in the XRD data. A number of other reflections, due either to the Si substrates [16] or impurities in the x-ray tube, are indicated in the figure and explained in the caption.

As mentioned above, a ZnO single crystal wafer was also measured with the same apparatus and its ZnO (002) reflection was observed at $2\theta \approx 34.45^{o}$. The (002) reflection full width at half maximum (FWHM), *c*-axis lattice spacing and out-of-plane coherence length (crystallite size, from the Scherrer equation) were measured for the PLD-grown ZnO seed layer (0.225^{o}, 0.520 nm and 35.30 nm, respectively), the VPT-grown ZnO nanorods (0.208^{o}, 0.519 nm and 38.11 nm, respectively) and the PLD-grown ZnO nanorods (0.198°, 0.521 nm, and 75.31 nm, respectively). The crystallinity of the nanorods is improved compared to the seed layers. The

value of *c*-axis lattice spacing for VPT- and/or PLD-grown ZnO nanorods is in excellent agreement with the value determined from the data from the ZnO wafer (i.e. 0.521 nm).

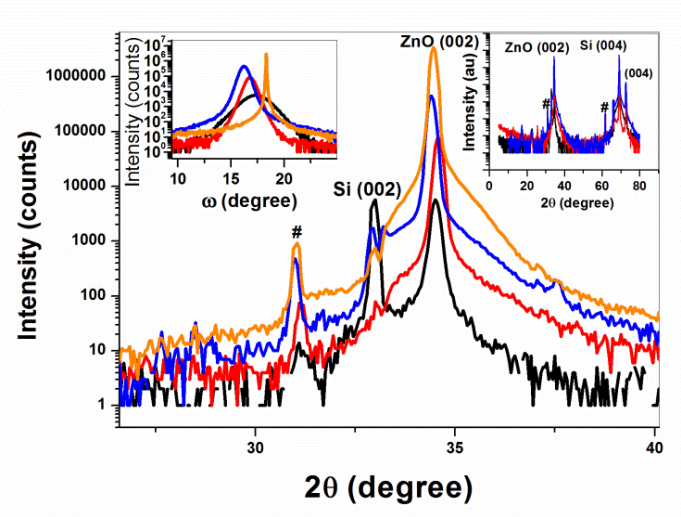

Figure 1. 2θ-ω XRD data for PLD-grown ZnO seed layers (black line), VPT-grown ZnO nanorods (red line), PLD-grown ZnO nanorods (blue line) and a ZnO wafer (orange line). The features marked with # are due to Cu K_β and tungsten L_α radiation from the X-ray tube, with the latter due to contamination. The left hand side inset shows the rocking curve (RC) data from the four samples around the ZnO (002) peak position. The right hand side inset shows the 2θ-ω data for the deposited samples over a broader 2θ angular range. Both insets use the same colours as in the main figure.

The left hand side inset of Fig. 1 shows rocking curve (RC) data for the (002) reflection of the PLD-grown ZnO seed layers, VPT-grown ZnO nanorods, PLD-grown ZnO nanorods and the ZnO wafer. The FWHM of the RCs for the PLD-grown ZnO seed layers, VPT-grown ZnO nanorods and PLD-grown ZnO nanorods are 2.16º, 0.84º and 0.76º, respectively. We note that our FWHM value for the RC for VPT-ZnO nanorods is much smaller compared to reports of

similar VPT-grown samples from Rajendra Kumar et al. and Li et al. who find FWHM values of ~ 2-2.8º and ~ 1.5º, respectively [6,7] and are comparable (albeit slightly larger than) the values for our PLD-grown ZnO nanorods. These data further indicate the highly textured nature (with *c*-axis orientation) of the nanorod deposits and the high crystalline quality of these materials compared to literature reports.

3.2 Surface morphologies

Fig. 2 shows the surface morphologies of the PLD-grown ZnO seed layers (Fig. 2a), VPT-grown ZnO nanorods (Fig. 2b, 2c and 2d) and PLD-grown ZnO nanorods (Fig. 2e and 2f). The PLD-grown ZnO seed layer is observed to be quite smooth and continuous. PLD-grown ZnO seed layers have been reported to be excellent substrates for the growth of high quality nanorods by Li et al. and Jie et al. [7,17]. Fig. 2b shows VPT-grown ZnO nanorods at a 30º tilt view while the inset shows a plan view of the same nanorods. Fig. 2c shows a higher magnification view of the individual VPT-grown nanorod morphology at the same 30º tilt view while the Fig. 2d shows 70º tilt view of these nanorods. These data show that the VPT-grown nanorods have excellent *c*-axis orientation normal to the substrate surface, which correlates well with the XRD analysis discussed above. Fig. 2c in particular shows that the VPT-grown nanorods are well separated (typically by some 100's of nm) and show smooth, facetted top and side surfaces, indicative of the underlying hexagonal crystalline symmetry. Previous TEM studies of VPT grown ZnO nanorods have shown that VPT-grown nanorods synthesized under similar conditions have extremely smooth surfaces and are crystalline throughout, consistent with the SEM data in Fig. 2 [8,9,18]. SEM data from PLD-grown ZnO nanorods at 30º tilt view is shown in Fig. 2e while the inset shows a top view of the same nanorods. Fig. 2f shows an 85º tilt view of these PLD-grown ZnO nanorods. Although an identical PLD-grown ZnO seed layer

was used for the growth of both VPT- and PLD-ZnO nanorods, the PLD-grown ZnO nanorods are very closely packed and the nanorod surfaces show evidence of considerable roughness, which is likely due to both the inhomogeneous sub-surface region of these nanostructures close to the nanorod surface, where a sub-surface transition region is seen from an inner crystalline region to an amorphous surface region as revealed by previous TEM studies [12], as well as proximity effects from neighbouring nanorods contacting each other during growth. Once again the data show that the PLD-grown nanorods have excellent *c*-axis orientation normal to the substrate surface, which again correlates well with the XRD analysis discussed above.

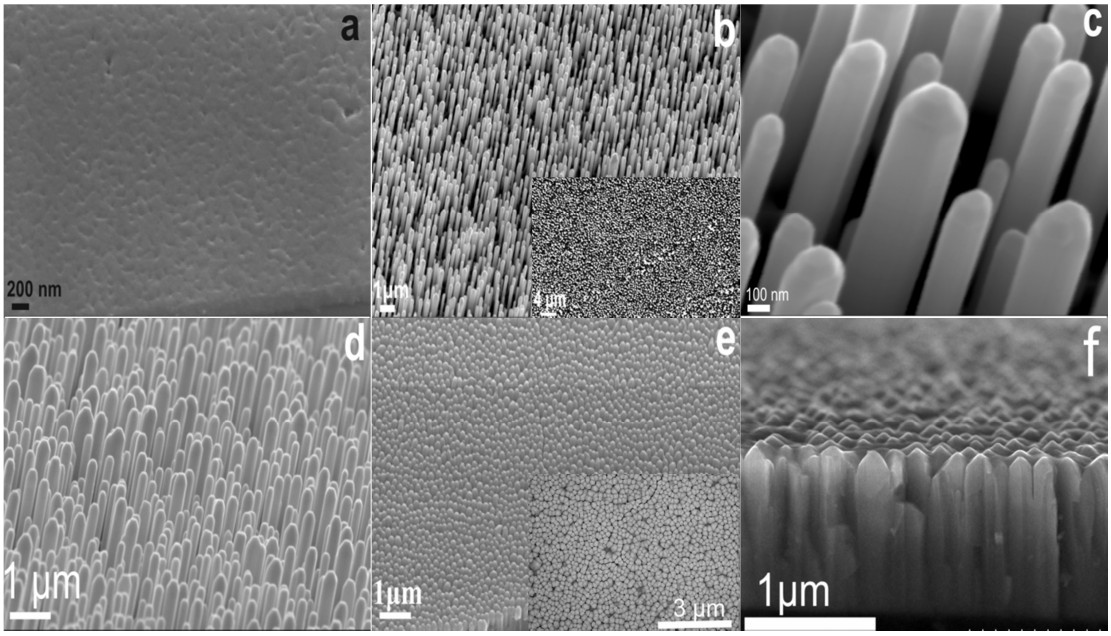

Figure 2. SEM data from the (a) PLD-grown ZnO seed layers at 30º tilt view, (b) VPT-grown ZnO nanorods at 30º tilt view, (c) an enlarged view of (b), and (d) the same VPT-grown ZnO nanorods at 70º tilt view, (e) PLD-grown ZnO nanorods at 30º tilt view, (f) the same PLD-grown

ZnO nanorods at 80º tilt view. The inset of (b) shows a plan view of (b) with a smaller magnification scale while the inset of (e) shows a plan view of (e).

The lengths and widths of the VPT-grown ZnO nanorods were extracted using 'Image J' software [19] and are in the range of 1.5 - 2 μm and ~ 175 - 200 nm, respectively. The same quantities for the PLD-grown ZnO nanorods are in the range of 0.9 - 1.2 μm and ~ 135 - 200 nm, respectively. The surface coverage density of the VPT-grown ZnO nanorods was measured to be ~ 18 per μm^2 (based on a count of ~ 75 nanorods in a 4 μm^2 region) and ~ 28 per μm^2 for the PLD-grown ZnO nanorods (based on a count of ~ 113 nanorods in a 4 μm^2 region, somewhat larger values than in previous works [6,7].

3.3 Optical properties

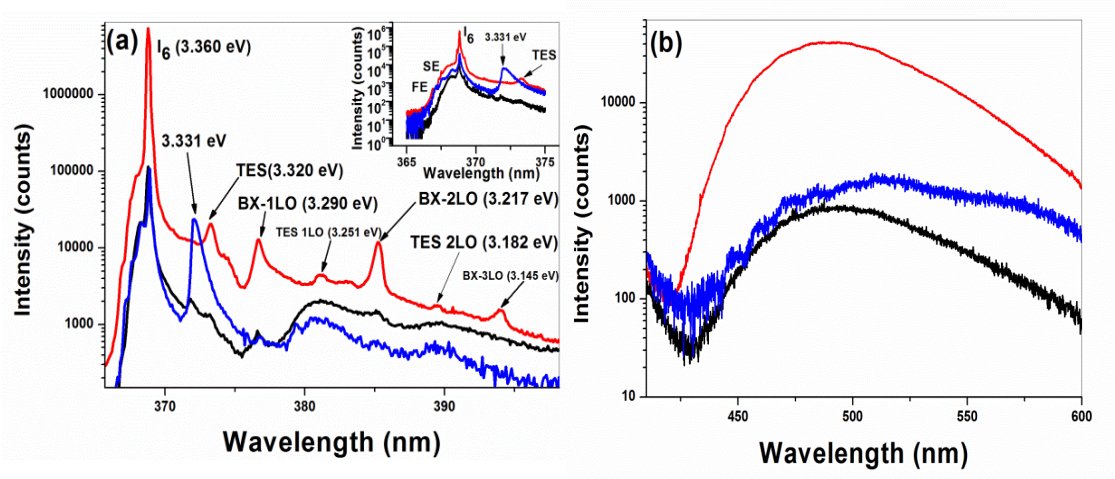

Figure 3. Low-temperature (13 K) PL spectra of PLD-grown ZnO seed layers (black lines), VPT-grown ZnO nanorods (red lines) and PLD-grown ZnO nanorods (blue lines): (a) near band

edge region, (b) visible region. Inset of (a) shows magnified view of surface exciton (SE) and free exciton (FE) spectral region.

Fig. 3a shows the near band edge emission region for all the deposited samples, which is dominated by the I_6 bound exciton (BX) line at 3.36 eV in all cases, which is attributed to Al impurities, as well as the surface exciton (SE) and free excitons (FE) for the three samples, which can be seen in the inset of Fig. 3a. FWHM values of the I_6 BX for the PLD-grown ZnO seed layers, VPT-grown ZnO nanorods and PLD-grown ZnO nanorods are 2.062 meV, 1.994 meV and 1.437 meV, respectively indicating the high optical quality of these samples. Two electron satellite (TES) and longitudinal optical (LO) replicas are normally observed in the highest optical quality materials and are located in the spectral region ~ 30-70 meV from the parent emissions. Such features are clearly seen for VPT-grown ZnO nanorods; we observe the TES of the I_6 line at 3.320 eV and its two LO replicas, TES 1LO and TES 2LO, at 3.251 eV and 3.182 eV, respectively. The LO replicas of the BX emission, such as BX-1LO, BX-2LO and BX-3LO are also clearly seen for the VPT-grown ZnO nanorods at 3.290 eV, 3.217 eV and 3.145 eV, respectively, and less clearly for the PLD-grown materials. The LO replicas in all cases are spaced ~ 72 meV apart, characteristic of the ZnO crystal. The PL intensity from the VPT-grown ZnO nanorods is much greater than both the PLD-grown ZnO seed layer and the PLD-grown nanorods in both the near band edge and visible spectral regions (the latter shown in Fig. 3b).

In the case of PLD-grown ZnO nanorods, a defect-related emission at 3.331 eV and its TES and LO replicas were also seen, as reported in our previous work [12], which is not seen in either the PLD-grown seed layer emission or the VPT-grown nanorod emission. The intensity of this emission is comparable to the BX emission in the same sample. This emission was first

reported in our previous report [12] and its origins investigated, using TEM and other studies of the nanorods involved. However the present study allows us to make comparisons with ZnO nanorod deposits grown by VPT, as well as with continuous ZnO film deposits. The data in Fig. 3 show that the 3.331 emission is seen only from the PLD-grown ZnO nanorods. Our previous study allowed us to tentatively assign the origin of this spectral feature to structural defects in the inhomogeneous sub-surface region close to the rough nanorod surface, where a sub-surface transition region from an inner crystalline region to an amorphous surface region is observed. This study adds considerable weight to this assignment since the feature is not seen in a continuous film (where the sub-surface transition region from a crystalline to an amorphous structure, seen for PLD-grown ZnO nanorods, is not present) deposited by PLD at similar temperatures, nor is it seen in VPT-grown nanorods also deposited at similar temperatures which are well separated and display very smooth, facetted surfaces, indicative of nanorod crystallinity continuing right to the nanorod surface. The emission is only seen from PLD-grown ZnO nanorods which are very closely packed and whose surfaces show evidence of considerable roughness, which is likely due to both the inhomogeneous sub-surface region of these nanostructures close to the nanorod surface, where a sub-surface transition region is seen from an inner crystalline region to an amorphous surface region [12], as well as proximity effects from neighbouring nanorods contacting each other during growth.

The totality of data from our present measurements allow us to confidently assign the 3.331 eV emission to recombination at structural defects with slightly different environments in the inhomogeneous sub-surface region, where the transition from a crystalline to an amorphous structure means a variety of defects environments are present in the outermost parts of the crystalline region, giving rise to a relatively large inhomogeneous line width. Our data show that

the appearance of this feature is intimately linked to the presence of an inhomogeneous sub-surface region in the nanorods, and that the absence of such inhomogeneous sub-surface regions (in continuous films such as the PLD-grown seed layer) or their replacement by fully crystalline nanorods with smooth, facetted surfaces (in the VPT-grown nanorod sample) leads to the complete disappearance of this feature.

4. Conclusions

We have successfully grown ZnO nanorods by both VPT and PLD on PLD-grown ZnO seed layers and have studied the structural, morphological and luminescent properties of the both types of nanorods as well as the underlying PLD-grown ZnO seed layers. XRD studies show that the VPT-grown and PLD-grown ZnO nanorods, as well as the PLD-grown seed layers are highly textured with *c*-axis orientation normal to the substrate plane. SEM images confirm this and further show that the VPT-grown ZnO nanorods are well separated with the nanorods spaced by distances of 100's nm, with smooth facetted top and side surfaces while PLD-grown ZnO nanorods are densely packed and show rough surfaces by comparison. Low temperature PL from all samples shows a dominant I_6 BX line, along with SE and FE emission in the near band edge region, while the VPT-grown nanorods clearly show TES and TES LO phonon replicas as well as LO replicas of the I_6 BX. These data reflect the high optical quality of the deposited material, in particular for the case of VPT-grown ZnO nanorods. In the near band edge spectrum from PLD-grown ZnO nanorods, a recently reported defect related emission was observed at 3.331 eV, which was not seen for either the PLD-grown seed layer or VPT-grown nanorod samples.

Overall, the present report allows us to confidently assign the 3.331 eV emission to recombination at structural defects in the sub-surface transition region from a crystalline to an

amorphous structure, and shows that the presence of such an inhomogeneous sub-surface region is crucial to the observation of this emission feature. Hence the present work contributes to an important increase in understanding of the different optically-active defects which contribute to the near-UV band edge photoluminescence (PL) in ZnO nanostructures and the relationship of these defects to the nanostructure morphology, which is crucial to the choice of the optimum growth parameters when targeting a particular application.

Acknowledgements

S. Inguva acknowledges the award of a postgraduate studentship from INSPIRE (Integrated Nanoscience Platform for Ireland). This INSPIRE-funded work was conducted under the framework of the Irish Government's Programme for Research in Third Level Institutions, Cycle 5, National Development Plan 2007-2013 with the assistance of the European Regional Development Fund. C. Gray acknowledges funding from an Irish Research Council Postgraduate Scholarship under the EMBARK Initiative.

References

[1] D.C. Kim, B.H. Kong, H.K. Cho, D.J. Park, J.Y. Lee, Effects of buffer layer thickness on growth and properties of ZnO nanorods grown by metalorganic chemical vapour deposition, Nanotechnology 18 (2007) 015603.

[2] X. Wang, C.J. Summers, Z.L. Wang, Large-Scale Hexagonal-Patterned Growth of Aligned ZnO Nanorods for Nano-optoelectronics and Nanosensor Arrays, Nano Lett. 4 (2004) 423-426.

[3] A.B. Djurisic, A.M.C. Ng, X.Y. Chen, ZnO nanostructures for optoelectronics: Material properties and device applications, Prog. Quant. Electron. 34 (2010) 191–259.

[4] Y. Shao, J. Yoon, H. Kim, T. Lee, W. Lu, Temperature Dependence of Electron Transport in ZnO Nanowire Field Effect Transistors, IEEE T. Electron Dev. 61 (2014) 625-630.

[5] D. Byrne, E. McGlynn, J. Cullen, M.O. Henry, A catalyst-free and facile route to periodically ordered and c-axis aligned ZnO nanorod arrays on diverse substrates, Nanoscale 3 (2011) 1675-1682.

[6] R.T. Rajendra Kumar, E. McGlynn, C. McLoughlin, S. Chakrabarti, R.C. Smith, J.D. Carey, J.P. Mosnier, M.O. Henry, Control of ZnO nanorod array density by Zn supersaturation variation and effects on field emission, Nanotechnology 18 (2007) 215704.

[7] C. Li, G. Fang, J. Li, L. Ai, B. Dong, X. Zhao, Effect of seed layer on structural properties of ZnO nanorod arrays grown by vapor-phase transport, J. Phys. Chem. C 112 (2008) 990-995.

[8] C. Li, G. Fang, Q. Fu, F. Su, G. Li, X. Wu, X. Zhao, Effect of substrate temperature on the growth and photoluminescence properties of vertically aligned ZnO nanostructures, J. Cryst. Growth. 292 (2006) 19-25.

[9] D. Zhao, C. Andreazza, P. Andreazza, J. Ma, Y. Liu, D. Shen, Buffer layer effect on ZnO nanorods growth alignment, Chem. Phys. lett. 408 (2005) 335-338.

[10] D.J. Park, D.C. Kim, J.Y. Lee, H.K. Cho, Synthesis and microstructural characterization of growth direction controlled ZnO nanorods using a buffer layer, Nanotechnology 17 (2006) 5238-5243.

[11] J. Song, S. Lim, Effect of seed layer on the growth of ZnO nanorods, J. Phys. Chem. C 111 (2007) 596-600.

[12] S. Inguva, S.K. Marka, R.K. Vijayaraghavan, E. McGlynn, Vadali V.S.S. Srikanth, J.-P. Mosnier, Crystalline ZnO/Amorphous ZnO Core/Shell Nanorods: Self-Organized Growth, Structure, and Novel Luminescence, J. Phys. Chem. C 119 (2015) 4848-4855.

[13] J.T.D. Ty, H. Yanagi, Electrochemical deposition of zinc oxide nanorods for hybrid solar cells, Jpn. J. Appl. Phys. 54 (2015) 04DK05.

[14] D. Byrne, E. McGlynn, M.O. Henry, K. Kumar, G. Hughes, A novel, substrate independent three-step process for the growth of uniform ZnO nanorod arrays, Thin Solid Films 518 (2010) 4489–4492.

[15] R.T. Rajendra Kumar, E. McGlynn, M. Biswas, R. Saunders, G. Trolliard, B. Soulestin, J.-R. Duclere, J.P. Mosnier, M.O. Henry, Growth of ZnO nanostructures on Au-coated Si: Influence of growth temperature on growth mechanism and morphology, J. Appl. Phys. 104 (2008) 084309.

[16] B.-H. Hwang, Calculation and measurement of all (002) multiple diffraction peaks from a (001) silicon wafer, J. Phys. D: Appl. Phys. 34 (2001) 2469-2474.

[17] J. Jie, G. Wang, Y. Chen, X. Han, Q. Wang, B. Xu, J.G. Hou, Synthesis and optical properties of well-aligned ZnO nanorod array on an undoped ZnO film, Appl. Phys. Lett. 86 (2005) 031909.

[18] D. Byrne, R.F. Allah, T. Ben, D.G. Robledo, B. Twamley, M.O. Henry, E. McGlynn, Cryst. Growth Des. 11 (2011) 5378–5386.

[19] C.A. Schneider, W.S. Rasband, K.W. Eliceiri, NIH Image to Image J: 25 years of image analysis, Nat. Methods 9 (2012) 671-675.